Computational microscopy beyond perfect lenses

Xingyuan Lu, ^{1,2} Minh Pham, ^{1,3} Elisa Negrini, ³ Damek Davis, ⁴ Stanley J. Osher, ³ and Jianwei Miao ^{1,*}

¹Department of Physics & Astronomy and California NanoSystems Institute, University of California, Los Angeles, California 90095, USA

²School of Physical Science and Technology, Soochow University, Suzhou 215006, China

³Department of Mathematics, University of California, Los Angeles, California 90095, USA

⁴School of Operations Research and Information Engineering, Cornell University, Ithaca, New York 14850, USA



(Received 18 June 2023; revised 13 December 2023; accepted 2 September 2024; published 13 November 2024)

We demonstrate that *in situ* coherent diffractive imaging (CDI), which leverages the coherent interference between strong and weak beams to illuminate static and dynamic structures, can serve as a highly dose-efficient imaging method. At low doses, *in situ* CDI can achieve higher resolution than perfect lenses with the point spread function as a delta function. Both our numerical simulations and experimental results demonstrate that combining *in situ* CDI with ptychography can reduce the required dose by up to two orders of magnitude compared with ptychography alone. We anticipate that computational microscopy based on *in situ* CDI can be applied across various imaging modalities using photons and electrons for low-dose imaging of radiation-sensitive materials and biological samples.

DOI: 10.1103/PhysRevE.110.054407

I. INTRODUCTION

The resolution of microscopy based on incoherent imaging is set by the point spread function (PSF) [1]. A microscope corresponding to an infiwith the PSF as a delta function, nite numerical aperture without aberration, would represent a perfect imaging system. The other important factor for any practical microscope is the illumination, that is, the number of particles (e.g., photons and electrons) per unit area and time required to form an image. With unlimited illumination, a phase-contrast microscope with perfect lenses would be the ultimate imaging system. However, many important systems, such as energy materials, catalysts, polymers, and biological samples, are very sensitive to x-rays or electrons, which are known as radiation damage effects [2–4]. work, we combine theoretical analysis, numerical simulations, and experimental validation to demonstrate that, at low doses, computational microscopy based on in situ coherent diffractive imaging (CDI) can outperform microscopy with perfect lenses. CDI is a lensless imaging technique with the resolution only limited by the wavelength and the highest frequency of the diffraction signal [5]. Over the years, CDI methods, such as conventional CDI, Bragg CDI, and ptychography, have been broadly implemented using synchrotron radiation, x-ray free-electron lasers, high harmonic generation, electron microscopy, and optical microscopy [6-26]. However, although CDI methods have overcome the resolution limit set by lenses, their application to radiation-sensitive samples remains challenging. An approach to improve CDI's dose efficiency is to incorporate strong scatterers near weakly scattering or biological samples [27–32]. More recently, numerical experiments have indicated that in situ CDI

significantly reduce the radiation dose by 1-2 orders of magnitude over conventional CDI [33]. However, the mathematical foundation of the radiation dose reduction in *in situ* CDI is unknown. Here, we use mathematical analysis, numerical simulations, and experimental evidence to demonstrate that *in situ* CDI could be the most dose-efficient imaging method, achieving higher resolution than microscopy with perfect lenses at low doses.

II. THEORY

In situ CDI takes advantage of the coherent interference from static and dynamic structures [Fig. 1(a)]. Let us define $_S$ and $_D$ as the Fourier transform of the static and dynamic structures, respectively, where, for simplicity, we omit the reciprocal space coordinates and time variable in the dynamic structure. We first consider conventional CDI without the static structure. The diffraction intensity of the dynamic structure is

$$I_0 \frac{r_e \lambda}{l_D \sigma_D}^2 |_D|^2 = I_D,$$
 (1)

where I_0 is the fluence (photons per unit area) of the incident wave on the dynamic structure, r_e is the classical electron radius, λ is the wavelength, I_D is the diffraction intensity (photons per pixel), and I_D and σ_D are the size and linear oversampling ratio of the dynamic structure [34], respectively. We rewrite Eq. (1) as

$$\tilde{D} = \frac{r_e \lambda^{\sqrt{I_0}}}{I_D \sigma_D} |D|^2 = I_D.$$
 (2)

Equation (2) can be represented as a circle in the complex plane [Fig. 2(a)]. Although Eq. (2) is a nonconvex problem, a unique solution [the red dot in Fig. 2(a)] can be solved by iterative phase retrieval algorithms [35], provided the fluence

^{*}Contact author: j.miao@ucla.edu

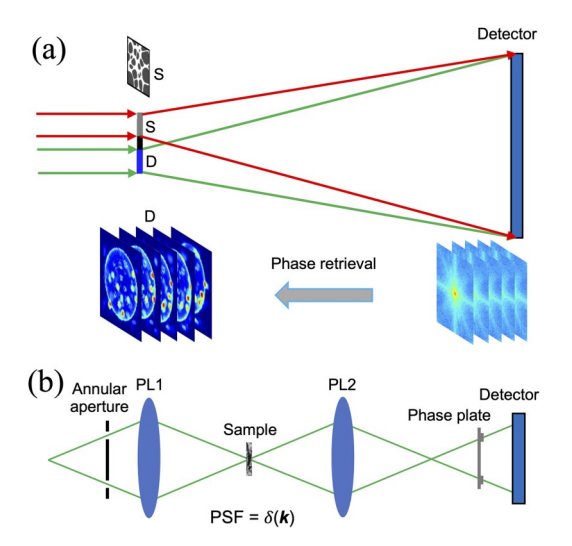


FIG. 1. Schematic of *in situ* coherent diffractive imaging (CDI) and phase-contrast microscopy with perfect lenses. (a) *In situ* CDI consists of static (S) and dynamic (D) structures that are coherently illuminated by strong and weak beams, respectively. Time-sequence diffraction patterns are collected from the coherent interference of the two beams by a detector, from which time-sequence phase images are reliably reconstructed by phase retrieval algorithms. (b) A perfect phase-contrast microscope with the point spread function (PSF) as a delta function, consisting of a source, annular aperture, first perfect lens (PL1), sample, second perfect lens (PL2), phase plate, and detector.

is sufficiently high and the oversampling condition is satisfied [34]. However, when the fluence is very low, the circle becomes an annulus with the width of the ring set by Poisson noise in the diffraction intensity [Fig. 2(b)]. The presence of very high noise will make iterative algorithms trapped in local minima instead of converging to the global minimum [35].

An approach to overcome this major limitation is *in situ* CDI (Fig. 1(a) and Fig. S1 in the Supplemental Material [36]), which is mathematically represented by

$$\frac{r_e \lambda^{\sqrt{l_1}}}{l_S \sigma_S} \quad {}_S + \frac{r_e \lambda^{\sqrt{l_0}}}{l_D \sigma_D} \quad {}_D^2 = I, \tag{3}$$

where I_1 is the fluence of the incident wave on the static structure with I_1 I_0 , I is the diffraction intensity, and l_S and σ_S are the size and linear oversampling ratio of the static structure [34], respectively. We rewrite Eq. (3) as

$$\tilde{S} = \frac{r_e \lambda^{\sqrt{I_1}}}{l_S \sigma_S} \quad |\tilde{S} + \tilde{D}|^2 = I.$$
 (4)

As $|\tilde{S}| = \tilde{D}|$, Eq. (4) can be represented by the intersection of a large circle and a small—annulus in the complex plane [Fig. 2(c)]. Due to very low relative noise in I, iterative phase retrieval algorithms can be used to find the global solution of $\tilde{S} + \tilde{D}$ [i.e., the red dot in Fig. 2(c)] instead of trapping in local minima. To mathematically solve Eq. (4), we define

$$\tilde{S} = F S = F_r S + i F_i S, \quad \tilde{D} = F D = F_r D + i F_i D,$$
 (5)

where F is the Fourier transform, S and D are the static and dynamic structures, and F_iS and F_iS are the real and imaginary parts of F S, respectively. Substituting Eq. (5) into Eq. (4) and

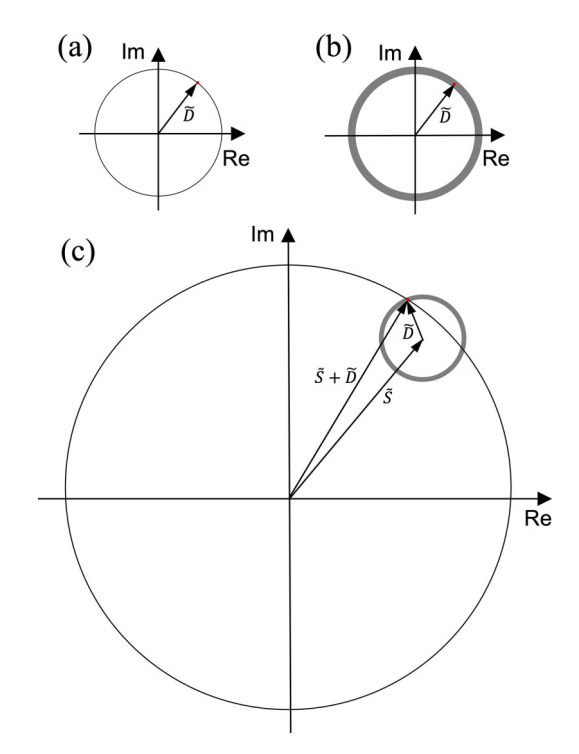


FIG. 2. Coherent diffractive imaging (CDI)-based computational microscopy in the complex plane. (a) In conventional CDI, the Fourier component of each pixel in reciprocal space represents a vector, \tilde{D} , confined in a circle. With low noise and the oversampling condition satisfied [34], the correct phase (red dot) can be recovered by phase retrieval algorithms. (b) With very high noise, the circle becomes an annulus, and phase retrieval algorithms are usually trapped in local minima instead of converging to the global minimum (red dot) [35]. (c) In *in situ* CDI, the coherent interference between a strong beam illuminating a static structure and a weak beam illuminating a dynamic structure produces a large circle in the complex plane, intersecting with a small annulus from the dynamic structure. Phase retrieval algorithms can quickly find the global minimum (red dot) instead of trapping in local minima as it becomes a convex problem (i.e., the intersected arc is almost a line segment).

ignoring the very small $|\tilde{D}|^2$ term, we have

$$F_r S F_r D + F_i S F_i D \approx \frac{1}{2} (I - |\tilde{S}|^2),$$
 (6)

where S can be accurately retrieved from the diffraction pattern due to the illumination of a high fluence on the static structure. Let us assume the array size of D and I to be $n \times n$ and $N \times N$, respectively. Since D is complex and I is real, with $N^2 \ge 2n^2$, there are more independent equations than unknown variables [36]. To solve Eq. (6), we convert it to the matrix form

$$AD = b$$

$$A = \operatorname{diag}(F_r S) F_r + \operatorname{diag}(F_i S) F_i \quad b = \frac{1}{2} (I - |\tilde{S}|^2), \quad (7)$$

where A is a diagonal matrix with dimension $N^2 \times N^2$, D has dimension $N^2 \times 1$ after padding with zeros, and b has dimension $N^2 \times 1$. Equation (7) can be solved by $D = (A^T A)^{-1} A^T b$, where A has independent columns, and superscripts T and -1 represent the transpose and inverse of a matrix. Although the

matrix $(A^TA)^{-1}A^T$ may have a large condition number, the solution can be stabilized by adding a damping term or l regularizer. Alternatively, Eq. (7) can be solved by the least-square method, $\min \frac{1}{2} AD^-b^2$, where D is constrained by a support. This becomes a convex problem and can be solved by optimization methods. Figure S2 in the Supplemental Material [36] shows specific examples of solving D using the above methods, with results comparable to those obtained through a traditional iterative phase retrieval algorithm.

III. SIMULATION RESULTS

To compare *in situ* CDI with a perfect imaging system, we simulate Zernike phase-contrast microscopy with perfect lenses (Fig. 1(b) and Supplemental Material [36]). In our numerical simulations, we first simulate a dynamic biological vesicle of protein complexes in water, consisting of 20 frames with a thickness of 100 nm and a pixel size of 11.4 nm (Video S1 and Table S1 in the Supplemental Material [36]). Figure S3(a)–S3(d) and Video S2(a) in the Supplemental Material [36] show representative noisy phase-contrast images of the biological vesicle using perfect lenses with fluences of 3.5×10^5 , 3.5×10^6 , 3.5×10^7 , and 3.5×10^8 photons/ μ m², respectively. To examine the effect of pixel size on resolution, we create biological vesicles with pixel sizes of 1, 5, and 10 nm and calculate their phase-contrast images with perfect lenses (Fig. S4 in the Supplemental Material [36]), indicating that, at these low doses, the resolution is limited by the dose instead of the pixel size.

We then use the time-varying biological vesicle as the dynamic structure and a 20-nm-thick Au pattern as the static structure (Fig. S1 in the Supplemental Material [36]). With an x-ray energy of 530 eV, we calculate time-sequence diffraction patterns from the complex exit waves of both the dynamic and static structures using Eq. (4), whereas the fluence on the static structure is 1 $\cdot 4 \times 10^{11}$ photons/ μ m², and the fluence on the dynamic structure varies from 3.5×10^5 , 3.5×10^6 , 3.5×10^7 , to 3.5×10^8 photons/ μ m². Poisson noise is added to the diffraction intensity calculated from both the static and dynamic structures. To reconstruct both the static and dynamic structure, we apply iterative phase retrieval algorithms to Eq. (4), which is more accurate than Eq. (8). We first reconstruct the static structure of the 20-nm-thick Au pattern from the diffraction patterns by combining the hybrid inputoutput algorithm [37] with shrinkwrap [38]. We then apply the static structure as a time-invariant constraint to retrieve the amplitudes and phases of the dynamic biological vesicle at different fluences using the generalized proximal smoothing algorithm [39]. We further improve the static structure during the phase retrieval of the time-sequence diffraction patterns [33], in which the illumination function of the incident wave can be incorporated if desired. Figure S4(e)-S4(h) and Video S2(b) in the Supplemental Material [36] show the representative phase images of in situ CDI with fluences of 3.5×10^5 , 3.5×10^6 , 3.5×10^7 , and 3.5×10^8 photons/ μ m², respectively. Using the Fourier ring correlation (FRC), we quantitatively compare the phase images between in situ CDI and perfect lenses (Fig. S4(i) and Table S2 in the Supplemental Material [36]), indicating that in situ CDI produces slightly higherresolution phase images than perfect lenses.

To study the effects of the sample thickness on perfect lenses and in situ CDI, we increase the thickness of the dynamic biological vesicle to 300 nm. Figures 3(a)-3(d) and Video S2(c) in the Supplemental Material [36] show the noisy phase-contrast images of perfect lenses with fluences of 3.5×10^5 , 3.5×10^6 , 3.5×10^7 , and 3.5×10^8 photons/ μ m², respectively. In comparison, we use the same phase-retrieval procedure of in situ CDI to reconstruct the amplitudes and phases of the dynamic biological vesicle, whereas the fluence on the dynamic structure varies from 3.5×10^5 , 3.5×10^6 , 3.5×10^7 , to 3.5×10^8 photons/ μ m² and the fluence on the static structure is fixed at 1.4×10^{11} photons/ μ m². Figures 3(e)-3(h) and Video S2(d) in the Supplemental Material [36] show the representative phase images of the biological vesicle. FRC comparisons indicate that in situ CDI produces higher-resolution phase images than perfect lenses (Fig. 3(i) and Table S2 in the Supplemental Material [36]). This improvement is due to the fundamental differences in the takes advantage of the coherent interference from all the pixels in the static and dynamic structures, from which a global solution of the complex wave is reconstructed. For a given fluence, increasing the sample thickness improves the signalto-noise ratio of the reconstructed images. This is in contrast to phase-contrast microscopy with perfect lenses, which forms images locally, that is, every pixel is independent of other pixels.

As most cellular structures are thicker than 500 nm, we increase the thickness of the dynamic biological vesicle to \mathcal{V} m. With such a thick sample, the weak phase approximation in Zernike phase-contrast microscopy no longer holds, but CDI methods do not have such a limitation. To reconstruct the thick biological sample by in situ CDI with the lowest possible dose, we reduce the x-ray fluences to 175×10^3 , 3.5×10^3 , 6.2×10^3 , and 7.7×10^3 photons/ μ m² (Fig. S5 in the Supplemental Material [36]). In particular, a fluence of 1.75×10^3 photons/ μ m² corresponds to 0.23 photon/pixel and a dose of 137.5 Gy. No conventional CDI method can perform successful phase retrieval under such an extremely low-dose condition. But in situ CDI successfully reconstructed the phase images of the biological vesicle in all these low-dose cases. This numerical experiment further confirms our mathematical analysis, that is, the arc of the larger circle intersected by the smaller circle in Fig. 2(c) is almost a line segment. Therefore, finding the correct phase [i.e., the red dot in Fig. 2(c)] becomes a linear problem, which can be solved by a linear solver as demonstrated in Fig. S2 in the Supplemental Material [36].

Next, we perform a numerical simulation on the potential dose reduction by combining *in situ* CDI with ptychography, termed low-dose CDI (LoCDI). Figure S6 in the Supplemental Material [36] shows a schematic of LoCDI, where strong and weak beams with E = 530 eV illuminate a static structure and biological sample, respectively. The static structure consists of a 20-nm-thick Au pattern and the biological sample is HeLa cells with sharp features and a thickness of 300 nm. A raster scan of 10×10 positions is performed on the static structure and the biological sample by the strong and weak beam, respectively. At each scan position, a coherent interference pattern is collected from the static structure and the biological sample. All numerical simulation parameters are

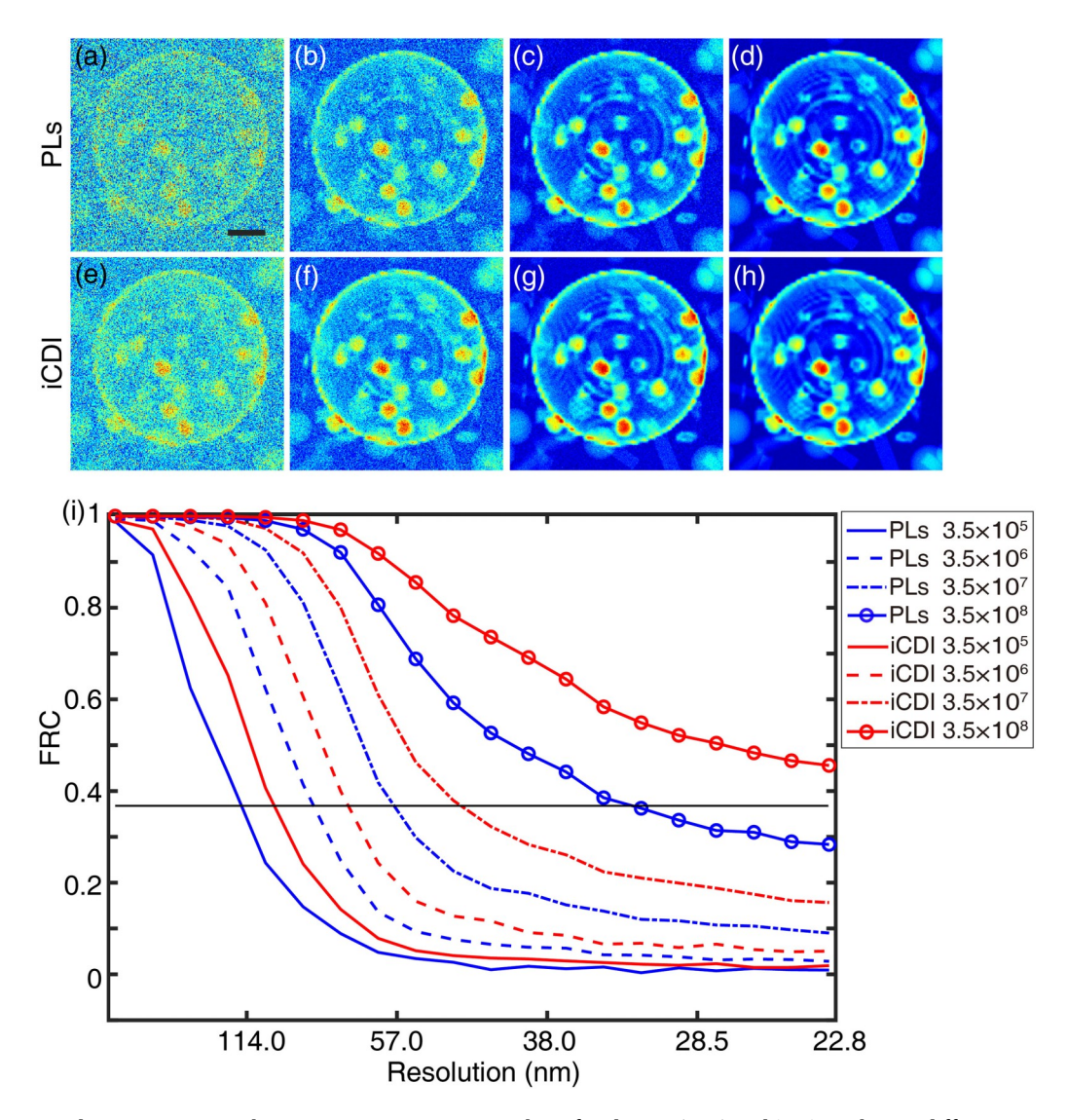


FIG. 3. Numerical experiments on phase-contrast microscopy with perfect lenses (PLs) and *in situ* coherent diffractive imaging (iCDI). (a)–(d) Representative images of a 300-nm-thick dynamic biological vesicle obtained by phase-contrast microscopy with perfect lenses using x-ray fluences of 3.5×10^5 , 3.5×10^6 , 3.5×10^7 , and 3.5×10^8 photons/ μ m², respectively, corresponding to doses of 2.75×10^4 , 2.75×10^5 , 2.75×10^6 , and 2.75×10^7 Gy, respectively. Scale bar: 500 nm. (e)–(h) The same images reconstructed by *in situ* CDI with x-ray fluences of 3.5×10^5 , 3.5×10^7 , and 3.5×10^8 photons/ μ m², respectively, and a fixed fluence of 1.4×10^{11} photons/ μ m² on the static structure. (i) Average Fourier ring correlation (FRC) curves of the 20-frame phase images obtained by perfect lenses and *in situ* CDI as a function of the x-ray fluence. The black line with FRC = 1/e indicates the resolution.

shown in Table S3 in the Supplemental Material [36]. From the 100 diffraction patterns, the static structure, biological sample, and probe function are simultaneously reconstructed by the extended ptychographic iterative engine (ePIE) [40] [Figs. 4(e)–4(h)]. For comparison, the phase images of the biological sample with perfect lenses under the same doses are shown in Figs. 4(a)–4(d). Quantitative comparisons using the FRC curves indicate that LoCDI produces superior phase images to perfect lenses at these doses (Fig. 4(m) and Table S2 in the Supplemental Material [36]). We also use ptychography to reconstruct the biological samples with the strong beam removed [Figs. 4(i)–4(l)]. FRC comparisons indicate that LoCDI can reduce the dose by two orders of magnitude over ptychography (Fig. 4(n) and Table S2 in the Supplemental Material [36]).

IV. EXPERIMENTAL RESULTS

To further validate our mathematical analysis and numerical simulation, we conduct a LoCDI experiment where a laser beam is split into two beams and a lens is used to separate the two beam paths near the focal plane [Fig. 5(a)]. One beam is attenuated by a filter, and the other is unattenuated. The two beams then illuminate two pinholes, each with a diameter of $100~\mu$ m, creating strong and weak probes. The separation between the two pinholes is set to 1 mm to avoid any interference between the two probes on the sample. The sample, a USAF resolution test pattern [Fig. 5(b)], is positioned immediately after the pinholes and raster scanned across the two probes. At each scan position, a diffraction pattern from the illumination of two probes is measured by a charge-coupled device, which has 1024×1024 pixels with a pixel size of $13~\mu$ m and is

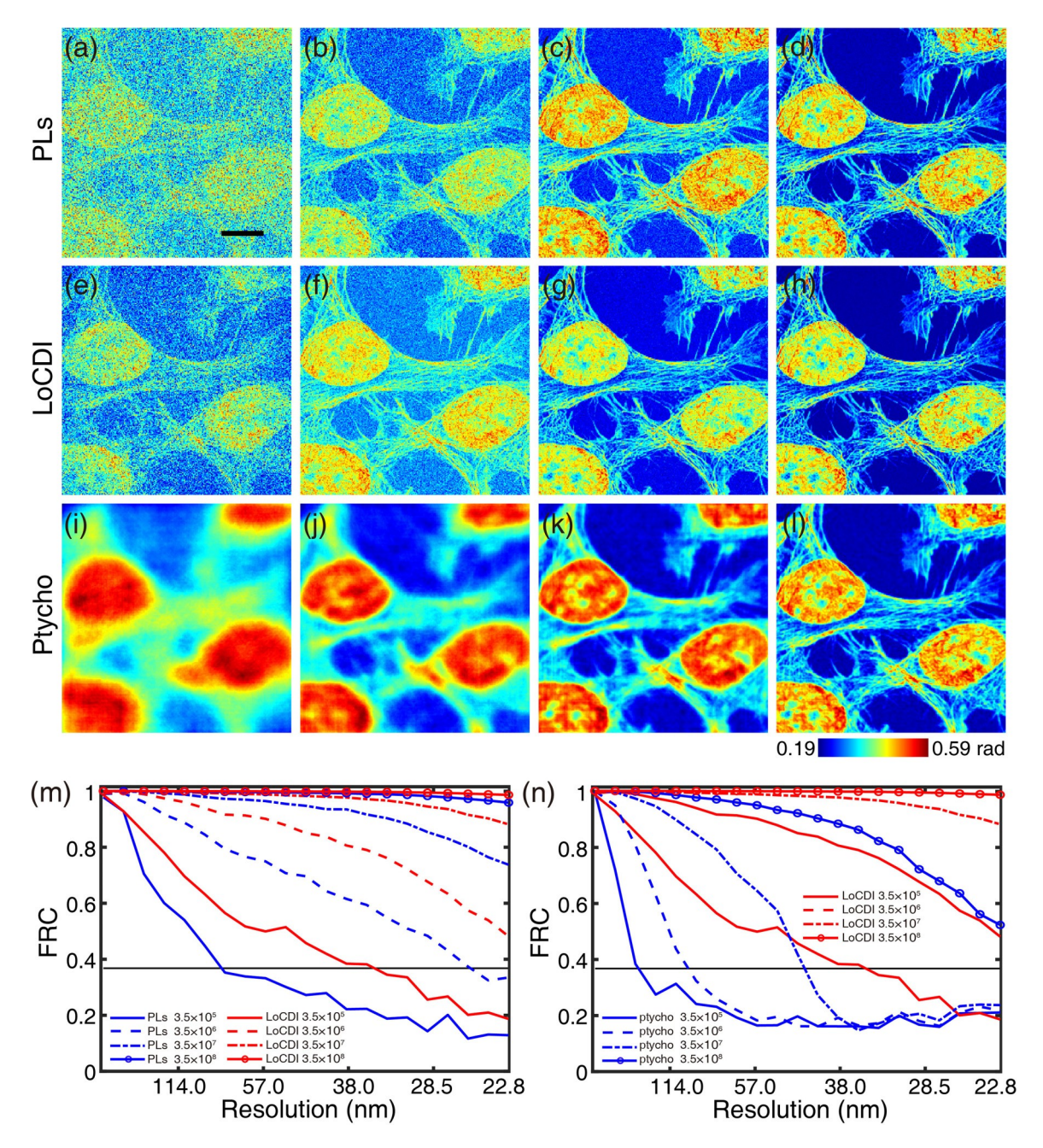


FIG. 4. Numerical simulation of the dose reduction with low-dose coherent diffractive imaging (LoCDI). (a)–(d) Phase-contrast images with perfect lenses using x-ray fluences of 3.5×10^5 , 3.5×10^6 , 3.5×10^7 , and 3.5×10^8 photons/ μ m², respectively. Scale bar: 500 nm. (e)–(h) Phase images of LoCDI with x-ray fluences of 35×10^5 , 3.5×10^6 , 3.5×10^7 , and 3.5×10^8 photons/ μ m² on the biological sample, respectively, and a fixed fluence of 14×10^{11} photons/ μ m² on the static structure. (i)–(l) Phase images of ptychography with the same x-ray fluences as those of LoCDI, but without the strong beam. (m) Fourier ring correlation (FRC) comparisons indicate that LoCDI is superior to phase microscopy with perfect lenses. (n) FRC comparisons with the ground truth of the biological sample indicate that LoCDI can reduce the dose by two orders of magnitude over ptychography with a fluence of 35×10^5 photons/ μ m².

placed 76.7 mm after the sample. For each data set, a total of 34×34 scan positions are conducted with an overlap ratio of 66%. By using different filters, we collect four datasets each with total fluences of $2 \cdot 2 \times 10^7$, $1 \cdot 7 \times 10^8$, $3 \cdot 7 \times 10^8$, and $3 \cdot 8 \times 10^9$ photons/mm², while the fluence on the strong probe was kept at $2 \cdot 2 \times 10^{10}$ photons/mm². Figures 5(c) - 5(f) shows the reconstructed images at four different fluences by ePIE. In comparison, we acquire four ptychographic datasets by blocking the unattenuated beam while keeping all other parameters

the same. Figures 5(g)-5(j) shows the reconstructions by ePIE with the same fluence on the sample. Quantitative comparison using the FSC curves indicates that LoCDI can reduce the dose by two orders of magnitude over ptychography (Fig. 5(k) and Table S2 in the Supplemental Material [36]).

By leveraging the coherent interference between strong and weak beams, which illuminate static and dynamic structures, respectively, *in situ* CDI emerges as a highly dose-efficient imaging method. Our numerical simulations indicate that

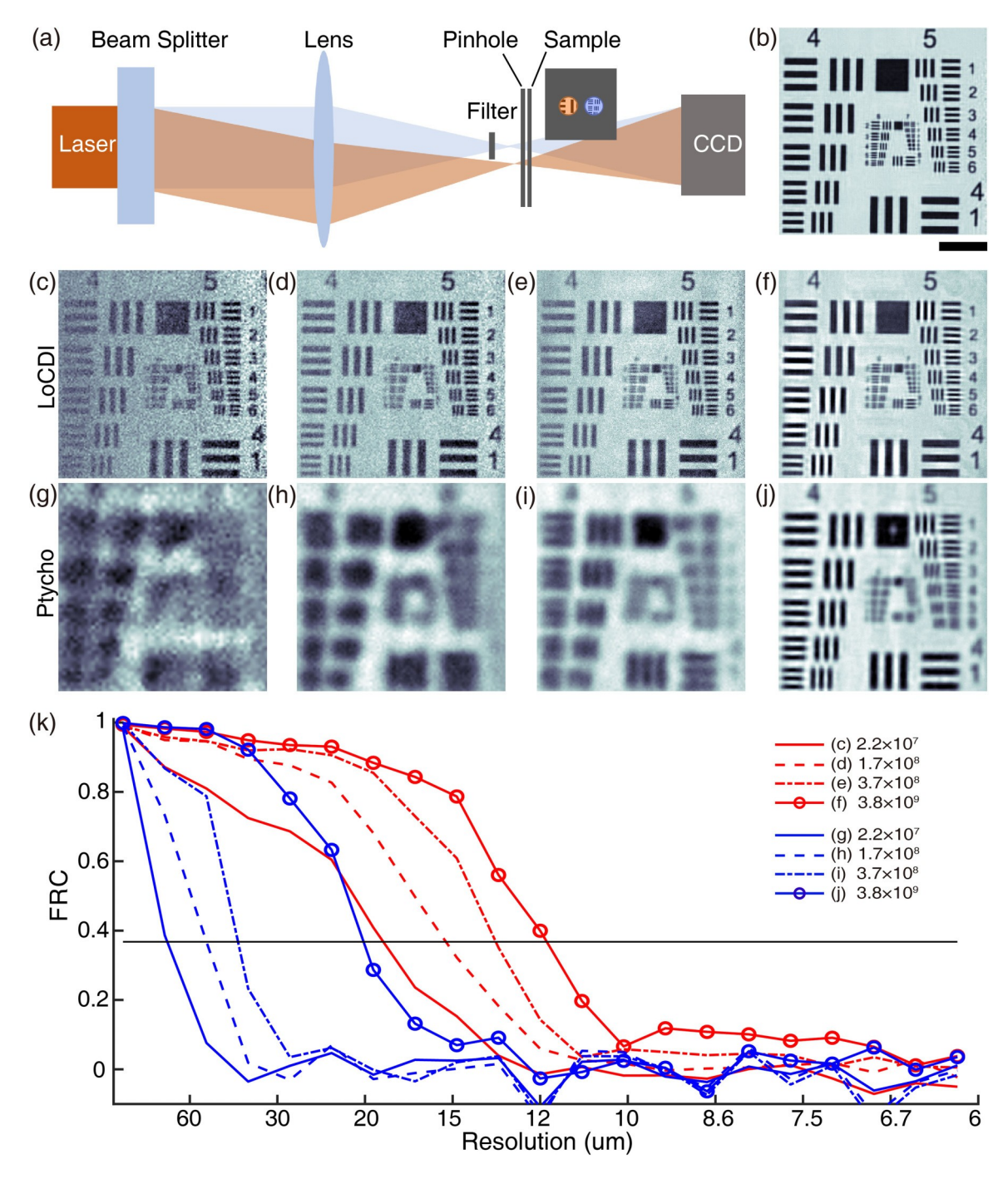


FIG. 5. Experimental demonstration of significant dose reduction with low-dose coherent diffractive imaging (LoCDI). (a) Schematic of the experimental setup using a laser with a wavelength of 532 nm (CCD: charge-coupled device). (b) The structure of a USAF resolution test pattern, obtained by a high-dose ptychography experiment. Scale bar: 200 μ m. (c)–(f) Reconstructed images with fluences of $2 \cdot 2 \times 10^7$, 1.7×10^8 , 3.7×10^8 , and 3.8×10^9 photons/mm², respectively, illuminating the sample (light blue), while the fluence of the unattenuated probe (brown) was kept at $2 \cdot 2 \times 10^{10}$ photons/mm². (g)–(j) Ptychographic reconstructions of the same sample with fluences of $2 \cdot 2 \times 10^7$, 1.7×10^8 , 3.7×10^8 , and 3.8×10^9 photons/mm², respectively, while the unattenuated beam (brown) was blocked. (k) Fourier ring correlation (FRC) curves of LoCDI and ptychographic reconstructions as a function of the fluences, which were calculated with the structure in (b).

in situ CDI not only achieves higher resolution than perfect lenses under low-dose conditions but also reduces the required dose by up to two orders of magnitude compared to ptychography. Since perfect lenses do not exist in nature, a direct experimental comparison with *in situ* CDI is unfeasible. Instead, we use ptychography as a reference technique to eval-

uate *in situ* CDI relative to the ideal performance of perfect lenses. Our experimental results confirm that *in situ* CDI can reduce the required dose by two orders of magnitude compared to ptychography, validating our numerical simulations. Moreover, by using the static structure as a time-invariant constraint to reconstruct the dynamic, time-variant structure,

in situ CDI can achieve high temporal resolution, limited only by the fluence and detector readout speed. Combined with coherent x-ray sources and bright electron sources, we anticipate that *in situ* CDI will become a powerful, dose-efficient imaging method for probing the structure and dynamics of a wide range of radiation-sensitive materials and biological samples.

ACKNOWLEDGMENTS

This work was supported by the U.S. Air Force Office Multidisciplinary University Research Initiative (MURI) program under Award No. FA9550-23-1-0281 and STROBE: A National Science Foundation Science and Technology Center

under Award No. DMR-1548924. M.P. and E.N. acknowledge support by the Simons Postdoctoral Program at IPAM and DMS1925919. D.D. acknowledges support from an Alfred P. Sloan Research Fellowship and NSF DMS Award No. 2047637.

X.L. and M.P. contributed equally to this work. J.M. directed the project; M.P., J.M., E.N., D.D., and S.J.O. discussed and/or carried out the mathematical analysis; X.L., M.P., E.N., and J.M. discussed and/or performed the numerical simulation; X.L. and J.M. contributed to the planning and execution of the optical experiment. J.M., X.L., and M.P. wrote the manuscript with input from E.N. All authors commented on the manuscript.

- [1] *Progress in Optics*, edited by E. Wolf (Elsevier, 2008), Vol. 51, p. 349.
- [2] R. Henderson, Q. Rev. Biophys. 28, 171 (1995).
- [3] M. R. Howells *et al.*, J. Electron Spectros. Relat. Phenom. **170**, 4 (2009).
- [4] M. Du and C. Jacobsen, Ultramicroscopy **184**, 293 (2018).
- [5] J. Miao, P. Charalambous, J. Kirz, and D. Sayre, Nature (London) **400**, 342 (1999).
- [6] J. Miao et al., Phys. Rev. Lett. 89, 088303 (2002).
- [7] D. Shapiro *et al.*, Proc. Natl. Acad. Sci. USA **102**, 15343 (2005).
- [8] M. A. Pfeifer et al., Nature (London) 442, 63 (2006).
- [9] H. N. Chapman et al., Nat. Phys. 2, 839 (2006).
- [10] J. M. Rodenburg et al., Phys. Rev. Lett. 98, 034801 (2007).
- [11] P. Thibault et al., Science 321, 379 (2008).
- [12] C. Song et al., Phys. Rev. Lett. 101, 158101 (2008).
- [13] I. Robinson and R. Harder, Nat. Mater. 8, 291 (2009).
- [14] K. Giewekemeyer et al., Proc. Natl. Acad. Sci. USA 107, 529 (2009)
- [15] Y. Nishino et al., Phys. Rev. Lett. 102, 018101 (2009).
- [16] H. N. Chapman and K. A. Nugent, Nat. Photon. 4, 833 (2010).
- [17] H. Jiang et al., Proc. Natl. Acad. Sci. USA 107, 11234 (2010).
- [18] M. M. Seibert et al., Nature (London) 470, 78 (2011).
- [19] G. Zheng, R. Horstmeyer, and C. Yang, Nat. Photon. 7, 739 (2013).
- [20] J. Miao, T. Ishikawa, I. K. Robinson, and M. M. Murnane, Science 348, 530 (2015).
- [21] D. F. Gardner et al., Nat. Photon. 11, 259 (2017).
- [22] M. Holler et al., Nature (London) 543, 402 (2017).

- [23] S. Gao et al., Nat. Commun. 8, 163 (2017).
- [24] Y. Jiang et al., Nature (London) 559, 343 (2018).
- [25] F. Pfeiffer, Nat. Photon. **12**, 9 (2018).
- [26] A. Rana et al., Nat. Nanotechnol. 18, 227 (2023).
- [27] S. Boutet *et al.*, J. Electron Spectros. Relat. Phenom. **166–167**, 65 (2008).
- [28] C. T. Putkunz et al., Phys. Rev. Lett. 106, 013903 (2011).
- [29] T. Y. Lan, P. N. Li, and T. K. Lee, New J. Phys. 16, 033016 (2014).
- [30] C. Kim et al., Opt. Express 22, 29161 (2014).
- [31] Y. Takayama et al., Sci. Rep. 5, 8074 (2015).
- [32] D. Noh et al., J. Phys.: Condens. Matter 28, 493001 (2016).
- [33] Y. H. Lo et al., Nat. Commun. 9, 1826 (2018).
- [34] J. Miao, D. Sayre, and H. N. Chapman, J. Opt. Soc. Am. A 15, 1662 (1998).
- [35] Y. Shechtman et al., IEEE Signal Proc. Mag. 32, 87 (2015).
- [36] See Supplemental Material at http://link.aps.org/supplemental/ 10.1103/PhysRevE.110.054407 for Supplemental figures, table, videos, and which includes Refs. [41–43].
- [37] J. R. Fienup *et al.*, Appl. Opt. **21**, 2758 (1982).
- [38] S. Marchesini *et al.*, Phys. Rev. B **68**, 140101 (2003).
- [39] M. Pham, P. Yin, A. Rana, S. Osher, and J. Miao, Opt. Express 27, 2792 (2019).
- [40] A. M. Maiden and J. M. Rodenburg, Ultramicroscopy 109, 1256 (2009).
- [41] F. Zernike, Science 121, 345 (1955).
- [42] M. Born and E. Wolf, *Principles of Optics*, 6th ed. (Pergamon Press, Oxford, 1980).
- [43] J. Kirz, C. Jacobsen, and M. Howells, Q. Rev. Biophys. **28**, 33 (1995).